New Journal of Physics
The open access journal at the forefront of physics

Deutsche Physikalische Gesellschaft DPG
IOP Institute of Physics

Published in partnership with: Deutsche Physikalische Gesellschaft and the Institute of Physics

OPEN ACCESS

RECEIVED
3 July 2022

REVISED
2 October 2022

ACCEPTED FOR PUBLICATION
6 October 2022

PUBLISHED
27 October 2022

PAPER

Biharmonic $(\omega, 2\omega)$ ionization of atoms by elliptically-polarized light. Carving the photoelectron angular distributions

S Fritzsche[1,2,3,*] and J Hofbrucker[1,2]

[1] Helmholtz-Institut Jena, D-07743 Jena, Germany
[2] GSI Helmholtzzentrum für Schwerionenforschung GmbH, D-64291 Darmstadt, Germany
[3] Theoretisch-Physikalisches Institut, Friedrich-Schiller-Universität Jena, D-07743 Jena, Germany
[*] Author to whom any correspondence should be addressed.

E-mail: s.fritzsche@gsi.de

Keywords: biharmonic ionization, two-photon ionization, atomic structure theory, circular dichroism, elliptical dichroism, photoelectron angular distribution

Abstract

The biharmonic $(\omega, 2\omega)$ photoionization of atomic inner-shell electrons opens up new perspectives for studying nonlinear light–atom interactions at intensities in the transition regime from weak to strong-field physics. In particular, the control of the frequency and polarization of biharmonic beams enables one to carve the photoelectron angular distribution and to enhance the resolution of ionization measurements by the (simultaneous) absorption of photons. Apart from its quite obvious polarization dependence, the photoelectron angular distributions are sensitive also to the (relative) intensity, the phase difference and the temporal structure of the incoming beam components, both at resonant and nonresonant frequencies. Here, we describe and analyze several characteristic features of biharmonic ionization in the framework of second-order perturbation theory and (so-called) ionization *pathways*, as they are readily derived from the interaction of inner-shell electrons with the electric-dipole field of the incident beam. We show how the photoelectron angular distribution and elliptical dichroism can be shaped in rather an unprecedented way by just tuning the properties of the biharmonic field. Since such fields are nowadays accessible from high-harmonic sources or free-electron lasers, these and further investigations might help extract photoionization amplitudes or the phase difference of incoming beams.

1. Introduction

The two-photon excitation and ionization of atoms and molecules is perhaps the simplest nonlinear light–matter interaction process that has been explored for pulses with a wide range of frequencies and intensities [1–6]. Apart from the simultaneous absorption of two photons from the same beam [7–9], the two-color photoionization [10, 11] as well as the ultra-fast response of gas targets to intense beams [12] has attracted much recent interest. Moreover, structured light beams have become feasible for photoionization experiments during the last years [13–15] and have enlarged our understanding of light–atom interactions [16, 17]. With the further advancement of free-electron lasers (FEL), in addition, the two- and multi-photon ionization of inner-shell electrons can now be explored also at extreme ultraviolet (XUV) and x-ray photon energies [18, 19], including the associated interplay of sequential, resonant and direct double ionization processes [20–23].

Further insight into the nonlinear light–atom interactions can be obtained by using biharmonic radiation fields that consist of two co-propagating beam components with multiples but of the *same* fundamental frequency ω, i.e. $m\omega + n\omega$ fields (m, n integers). At optical frequencies, for example, such biharmonic fields have been applied to create and control electron vortices [24, 25] or to generate

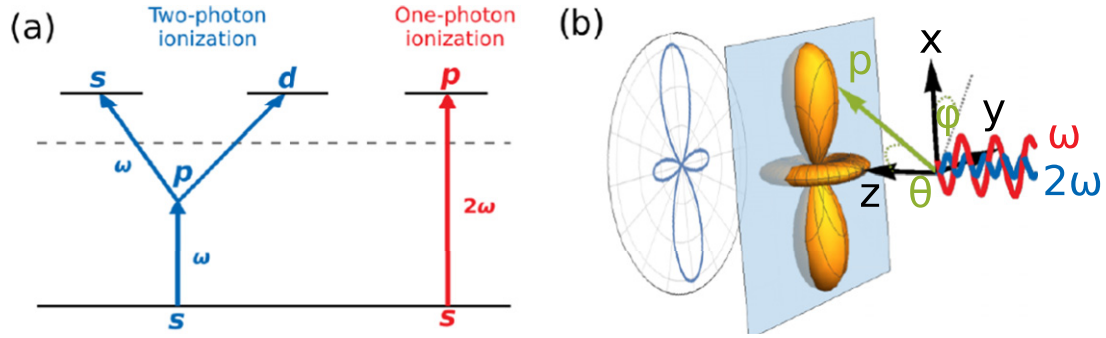

Figure 1. Biharmonic $(\omega, 2\omega)$ ionization of 1*s* inner-shell electrons. (a) The (nonrelativistic) one-photon $s \to p$ ionization pathway for the absorption of a photon with frequency 2ω (red arrow) and the two-photon $s \to p \to s$ and $s \to p \to d$ pathways for photons with frequency ω (blue arrows) generally interfere with each other and give rise to the biharmonic ionization of atoms as well as to all related observables of the emitted electron and/or photoion. (b) Typical choice of coordinates, in which the quantization (or *z*-) axis is taken along the propagation, and the *x*-axis along the main polarization axis of the incident beam. For this choice, the distribution of photoelectrons is characterized by the spherical angles (ϑ, φ) and will be displayed below either as three-dimensional distribution or just two-dimensional polar plots within the *x*–*y* polarization plane (light blue).

circularly-polarized high-harmonic fields [26–28]. At XUV photon energies, these biharmonic beams can be generated today at FEL owing to the high coherence of the individual harmonics at these facilities [29]. First pioneering experiments with linearly-polarized biharmonic and XUV beams were performed with helium and neon and have shown, that the one- and two-photon ionization amplitudes as well as the phases of the outgoing photoelectrons can be extracted from the measured angular distributions [29]. Furthermore, it has been demonstrated that the absolute phase between bichromatic XUV beam components can be derived with reasonable accuracy from the observed angular distributions, if combined with a few calculated parameters [30, 31].

In atomic physics, the term *biharmonic* ionization is often used in order to refer to the (single-electron) photoionization of atoms by biharmonic $(m\omega, n\omega)$ fields. For the sake of simplicity, we here consider the biharmonic $(\omega, 2\omega)$ ionization that makes use of the fundamental frequency ω and its second harmonic. For an atom in its initial state $|\alpha_{\rm i}\mathbb{J}_{\rm i}M_{\rm i}\rangle$, the (simultaneous) absorption of either *two* photons of frequency ω or *one* photon with frequency 2ω then leads to photoions in the final states $|\alpha_{\rm f}\mathbb{J}_{\rm f}M_{\rm f}\rangle$ and free electrons $|\mathbf{p}_e m_e\rangle$,

$$|\alpha_{\rm i}\mathbb{J}_{\rm i}M_{\rm i}\rangle + \left\{ \begin{array}{c} 2\cdot(\hbar\omega) \\ 1\cdot(2\hbar\omega) \end{array} \right\} \to |\alpha_{\rm f}\mathbb{J}_{\rm f}M_{\rm f}\rangle + |\mathbf{p}_e m_e\rangle,$$

where $\mathbb{J} \equiv J^P$ refers to the total angular momentum J and parity P, M to the projection of the angular momentum upon the quantization axis, and α to all other quantum numbers that are needed for specifying the fine-structure of the ions uniquely. For 1*s* inner-shell electrons, for example, its interaction with the electric-dipole ($E1$) components from such a biharmonic field will typically cause the photoelectron to leave the photoion in a partial wave with well-defined orbital angular momentum ℓ. As readily understood from perturbation theory, the photoelectron leaves the ion in a *p*-wave for the absorption of one photon with frequency 2ω, or a *s*- and *d*-wave ($\ell = 0, 2$) for the absorption of two $E1$ photons with frequency ω. Hereby, the partial wave with the highest angular momentum often appears to be dominant in single- and multi-photon ionization processes. Below, we shall therefore use the notation of $s \to p$ one-photon or, respectively, $s \to p \to s$ and $s \to p \to d$ two-photon pathways in order to analyze and explain many features as they are observed in biharmonic ionization experiments. Figure 1 schematically displays the pathways in the biharmonic $(\omega, 2\omega)$ ionization of 1*s* inner-shell electrons, and which are determined entirely by the well-known electric-dipole selection rules. Apart from the individual contributions of these three pathways, however, the photoelectron angular distribution is affected also by the interference of the associated ionization amplitudes. Until the present, the biharmonic ionization of atoms by $(\omega, 2\omega)$ fields has been mainly explored within the strong-field regime, for instance, by applying optical or infrared laser frequencies [32–34].

In practice, the nonlinear interaction of biharmonic fields with atoms has been *seen* (and explored) so far mainly in the circular dichroism and the photoelectron angular distribution. Here, a *dichroism* generally refers to (normalized) differences in the emitted electron distributions, if the handedness of the incident light beam is *reversed*, for instance from left-to right-circularly polarized light [35]. Similarly, the elliptical dichroism (ed) arise from a flip of the circular polarization component of a beam and has been utilized, for instance, in order to extract the degree of polarization of the incident beam itself [36] or its optical activity

in selected metamaterials [37]. In addition, the ed has been studied also in the above-threshold ionization of noble gases by elliptically polarized light [38, 39] and for investigating the structure of chiral molecules [40].

In this work, we describe the biharmonic $(\omega, 2\omega)$ ionization of neutral atoms within the single active-electron approximation and the framework of second-order perturbation theory. To this end, we first discuss the one- and two-photon ionization amplitudes and total cross sections separately, before we shall combine them in order to unveil the characteristic features of the biharmonic $(\omega, 2\omega)$ ionization. For the sake of illustration, we shall consider especially the 1*s* photoionization of atomic neon which is known to be well predicted within the single-active electron approximation. Emphasis is placed on how the frequency and polarization of the biharmonic beam affect the distribution of the emitted photoelectrons. To clearly distinguish the different contributions to the photoelectron distribution, we derive and explain in section 2 how the combined one- and two-photon amplitudes lead to a strong angular dependence (dichroism) of the emitted electrons. In section 3, we then discuss the energy dependence and angular distribution of neon 1*s* photoelectrons as well as their circular and ed. We briefly also consider the biharmonic $(m\omega, n\omega)$ multi-photon ionization by circularly-polarized light, though further details will need to be worked out to thoroughly account for all the different pathways in such multi-photon ionization processes. Finally, a short summary and conclusions are given in section 4. Atomic units ($m_e = \hbar = e^2/4\pi\varepsilon_0 = 1$) are used throughout the paper unless stated otherwise.

2. Theoretical background

2.1. Biharmonic light fields

Biharmonic fields are generally formed as superposition of two beam components with different color, polarization, and sometimes even of different pulse structure. For the sake of simplicity, we here consider the superposition of two vector potentials, one with fundamental frequency ω and another from its second harmonic

$$\mathbf{A}(\mathbf{r}, t) = A_0^{(\omega)} \mathbf{A}^{(\omega)}(\mathbf{r}, t) + \mathrm{e}^{\mathrm{i}\Phi} A_0^{(2\omega)} \mathbf{A}^{(2\omega)}(\mathbf{r}, t), \tag{1}$$

both propagating along the quantization axis, $\mathbf{k} \| \mathbf{e}_z$. Here, we clearly distinguish the fields amplitudes (intensities) $A_0^{(n\omega)} (n = 1, 2)$ right from the beginning from the spatially and time-dependent vector potentials, which then take the form

$$\mathbf{A}^{(n\omega)}(\mathbf{r}, t) = \boldsymbol{\epsilon}^{(n\omega)}\, \mathrm{e}^{-\mathrm{i}n\omega t + \mathrm{i}\mathbf{k}^{(n\omega)}\cdot\mathbf{r}}. \tag{2}$$

Obviously, the field amplitude $A_0^{(n\omega)}$ determine both, the flux $F^{(n\omega)} = \left(A_0^{(n\omega)}\right)^2$ and the intensity $I^{(n\omega)} = n\omega F^{(n\omega)} = n\omega \left(A_0^{(n\omega)}\right)^2$ of the corresponding component. Moreover, the phase shift between the two beams is given by Φ, while $\boldsymbol{\epsilon}^{(n\omega)}$ denotes the polarization vector of each component and is typically parametrized within the helicity basis $\mathbf{e}_\pm$ by means of the ellipticity $\epsilon^{(n\omega)}$ as

$$\boldsymbol{\epsilon} = \frac{\mathbf{e}_{-1}[1 - \epsilon] - \mathbf{e}_{+1}[1 + \epsilon]}{\sqrt{2[1 + \epsilon^2]}}. \tag{3}$$

The ellipticity of each beam component can take values in the range $-1 \leqslant \epsilon^{(n\omega)} \leqslant 1$, including left-circularly ($\epsilon = 1$), linearly ($\epsilon = 0$) and right-circularly ($\epsilon = -1$) polarized light, respectively. Vice versa, the degree of linear and circular polarization is then given by $P_\mathrm{l} = \frac{\epsilon^2 - 1}{\epsilon^2 + 1}$ and $P_\mathrm{c} = \frac{2\epsilon}{\epsilon^2 + 1}$. For present-day FEL facilities, moreover, the emitted pulses can often be assumed as (infinitely) long [30, 41–43] and, hence, modeled within the long-pulse approximation. In this approximation, the one- and two-photon ionization processes are simply described within lowest-order perturbation theory by using the transition amplitudes from below.

The *n*-photon transition amplitudes can be further simplified, if the photon field $\mathbf{A}^{(n\omega)}(\mathbf{r})$ is decomposed into the multipole components

$$\mathbf{A}^{(n\omega)}(\mathbf{r}) = 4\pi \sum_{LMp} i^{L-p} [\boldsymbol{\epsilon}^{(n\omega)} \cdot \mathbf{Y}_{LM}^{(p)*}(\hat{\mathbf{k}})] \mathbf{a}_{LM}^{(p)}(n\omega, \mathbf{r}), \tag{4}$$

which transform like spherical tensors of rank L, and where $p = 1$ refers to the electric and $p = 0$ to magnetic multipoles. We shall use this decomposition of the vector potentials into multipole fields in order to expand the one- and two-photon transition amplitudes below into (generalized) angular coefficients and radial integrals, and which are directly associated with the pathways mentioned above.

2.2. One-versus two-photon ionization of atoms

The (one-photon) ionization of atoms has been studied extensively since the use of the very first synchrotrons. Apart from energy-dependent cross sections, the angular distribution and (multiple) inner-shell resonances in the photoelectron spectra have attracted great interest, along with their polarization dependence. Not much need to be said about the theory of photoionization which has been described elsewhere [44, 45], even if detailed predictions about photoabsorption and photoelectron spectra still remain a challenge for atomic theory [46, 47].

In atoms with complex valence-shell structure, the absorption of a sufficiently energetic photon typically leads to the $n\ell$ inner-shell ionization of an electron in state $|n\ell m\rangle$ with binding energy ε_b and the release of a photoelectron with well-defined momentum $\mathbf{p}$ that can be expanded into partial waves (cf figure 1)

$$|\mathbf{p}\rangle = \sum_{\ell' m'} i^{\ell'}\, \mathrm{e}^{-\mathrm{i}\delta_{\ell'}} |\varepsilon' \ell' m'\rangle Y^*_{\ell' m'}(\vartheta, \varphi).$$

In this expansion, $|\varepsilon' \ell' m'\rangle$ are single-electron (partial) waves of well-defined energy $\varepsilon' \approx \omega - \varepsilon_b$[4], and where we use primed quantum numbers to refer to the final state of the (photo-) electron. Here, $\delta_{\ell'}$ denotes the scattering phase of the partial wave and $Y_{\ell' m'}(\vartheta, \varphi)$ a spherical harmonic that refers to the direction of the emitted electron. Since, moreover, the radiation field itself does not couple to the spin of the electron, the electric-dipole amplitudes can be characterized by just the $\ell \to \ell' = \ell \pm 1$ single-step pathways owing to the interaction of the photoelectron with the electric-dipole component of the incident light field.

In this (single) active-electron approximation, the one-photon ionization transition amplitude for the absorption of a photon with frequency 2ω is given by:

$$\begin{aligned} M^{(2\omega)}(n\ell m) &= \left\langle \mathbf{p} \middle| \mathbf{p} \cdot \mathbf{A}^{(2\omega)} \middle| n\ell m \right\rangle \\ &= 4\pi \sum_{\ell' m'} (-i)^{\ell'}\, \mathrm{e}^{\mathrm{i}\delta_{\ell'}}\, Y_{\ell' m'}(\vartheta, \varphi) \sum_{LMp} i^{L-p} [\boldsymbol{\epsilon}^{(2\omega)} \cdot \mathbf{Y}^{(p)}_{LM}] \\ &\quad \times \left[\ell'\right]^{-1/2} \langle \ell' m', LM | \ell m \rangle \left\langle \ell' \middle\| C^{(L)} \middle\| \ell \right\rangle U^{(pL)}(n\ell \to \ell'), \end{aligned} \tag{5}$$

and where the radial wave function of the $n\ell$ active electron only occurs in the (radial) amplitudes $U^{(pL)}(n\ell \to \ell')$. This decomposition therefore nicely reveals in the electric-dipole approximation the (single-step) ionization pathways $\ell \to \ell' = \ell \pm 1$ of the emitted photoelectron, and which then characterize also all the associated—angle-differential and total—one-photon cross sections. In addition, we shall often omit the initial shell n and the free-electron energy ϵ' in our discussion below as they are readily determined by energy conservation from the observed photoelectrons. Further (non-dipole) ionization pathways $\ell' = \ell \pm 2, \ldots$ are in principle possible but are strongly suppressed even at high photon energies. Although a good bulk of literature exists today on non-dipole contributions to the (one-photon) ionization of atoms [48–50], they are usually negligible for all multi-photon measurements owing to their present-day uncertainties.

An analog approximation (and discussion) also applies for the two-photon ionization pathways $\ell \to \ell' = \ell \pm 1 \to \ell'' = \ell, \ell \pm 2$. In this two-photon absorption process, the photoelectron leaves the ion with kinetic energy $\varepsilon \approx \hbar\omega_1 + \hbar\omega_2 - \varepsilon_b$ due to the *simultaneous* interaction with two photons. Experimentally, this ionization has been explored with photons from the same source ($\omega_1 = \omega_2 \equiv \omega$) or with photons of different frequency ($\omega_1 \neq \omega_2$), sometimes called two-color ionization. A particular intriguing two-color ionization process is the biharmonic $(\omega, 2\omega)$ photoionization ($\omega \equiv \omega_1 = \omega_2/2$). The associated two-photon ionization amplitude for the absorption of photons with frequency ω makes the nonlinear interaction of atomic electrons with the radiation field explicit in second-order perturbation theory, where it just simplifies to a product of (single-electron) amplitudes

$$\begin{aligned} M^{(\omega)}(n\ell m) &= 16\pi^2 \sum_{\ell'' m''} (-i)^{\ell''}\, \mathrm{e}^{\mathrm{i}\delta_{\ell''}}\, Y_{\ell'' m''}(\vartheta, \varphi) \sum_{L_1 M_1 p_1} \sum_{L_2 M_2 p_2} \sum_{l' m'} i^{L_1 - p_1 + L_2 - p_2} \left[\ell', \ell''\right]^{-1/2} \\ &\quad \times \left[\boldsymbol{\epsilon}^{(\omega)} \cdot \mathbf{Y}^{(p_1)}_{L_1 M_1}\right] \left[\boldsymbol{\epsilon}^{(\omega)} \cdot \mathbf{Y}^{(p_2)}_{L_2 M_2}\right] \langle \ell'' m'', L_2 M_2 | \ell' m' \rangle \langle \ell' m', L_1 M_1 | l m \rangle \\ &\quad \times \left\langle \ell'' \middle\| C^{(L_2)} \middle\| \ell' \right\rangle \left\langle \ell' \middle\| C^{(L_1)} \middle\| \ell \right\rangle U^{(p_1 L_2, p_2 L_2)}(n\ell \to \ell' \to \ell''). \end{aligned} \tag{6}$$

This two-photon amplitude includes a summation over the complete (single-) electron spectrum $\{(n', \ell', m')\}$ and over both, the occupied and unoccupied states of the target atoms. A detailed derivation of

[4] The $\approx$ symbol is used here and below to indicate that the observed electron energies are still weakly affected by the widths and intensity of the incident beam as well as the fine-structure of the target atoms.

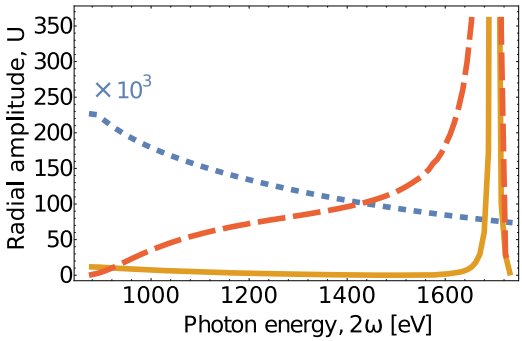

Figure 2. One- and two-photon (radial) amplitudes for the photoionization of neon 1*s* electrons as function of the photon energy. Results are shown for the $U^{(E1)}$ $(1s \to p)$ one-photon amplitude (blue dotted line) as well as the $U^{(E1,E1)}$ $(1s \to p \to s)$ (yellow solid line) and $U^{(E1,E1)}$ $(1s \to p \to d)$ (orange dashed line), respectively. Here, the one-photon integral $U^{(E1)}$ $(1s \to p)$ has been multiplied by a factor 10^3 to make it visible. See text for further discussion.

the two-photon amplitude $M^{(\omega)}$ $(n\ell m \to \ell' \to \ell'')$ has been given in reference [51]. Note that there is again just *one* amplitude for each pathway of the outgoing electron, and which reduces to an associated two-dimensional radial integral (radial amplitude), once the integration over all angular coordinates has been performed algebraically. For the biharmonic $(\omega, 2\omega)$ ionization of neon 1*s* electrons, figure 1 displays the E1 allowed one-photon $s \to p$ (red) as well as the two-photon $s \to p \to s$ and $s \to p \to d$ (blue) pathways that together determine entirely the electron emission.

Figure 2 illustrates the one- and two-photon amplitude for the ionization of neon 1*s* electrons as function of the incoming photon energy. Results are shown for the radial $U^{(E1)}$ $(1s \to p)$ one-photon amplitude (equation (5)) as well as the $U^{(E1,E1)}$ $(1s \to p \to s)$ and $U^{(E1,E1)}$ $(1s \to p \to d)$ two-photon amplitudes (equation (6)), respectively. Here, the one-photon amplitude $U^{(E1)}$ $(1s \to p)$ has been multiplied by a factor 10^3 in order to make it visible in this graph. The one-photon radial amplitude $U^{(E1)}$ $(1s \to p)$ is much smaller in magnitude, when compared with $U^{(E1,E1)}$ $(1s \to p \to d)$, due to their different origin in perturbation theory. While the (total) one-photon ionization amplitude typically decreases with increasing photon energy, the two-photon radial amplitudes are resonantly enhanced near to the $1s \to 2p$ excitation energy at ∼825 eV photon energy, i.e. for $2\omega \approx 1650$ eV.

2.3. Total and angle-differential biharmonic ionization rate

The one- and two-photon amplitudes from above serve as natural building blocks in order to express the total ionization probability and angle-differential cross sections for emitting an electron into the solid angle $\mathrm{d}\Omega = \sin\vartheta\, \mathrm{d}\vartheta\, \mathrm{d}\varphi$. For the biharmonic $(\omega, 2\omega)$ ionization, the angle-differential ionization rate is given by

$$\frac{\mathrm{d}W^{(\omega,2\omega)}}{d\Omega} = \sum_m \left| K^{(\omega)} M^{(\omega)}(nlm) + K^{(2\omega)} M^{(2\omega)}(nlm) \right|^2, \tag{7}$$

where the contributions of the one- and two-photon ionization (pathways) are determined by the weight factors $K^{(\omega)} = \frac{(2\pi)^{3/2}\alpha F^{(\omega)}}{\omega}$ and $K^{(2\omega)} = \sqrt{\frac{2\alpha\pi^2 F^{(2\omega)}}{\omega}}$ owing to the fluxes $F^{(\omega)}$ and $F^{(2\omega)}$ of the two beam components. These weight factors can be derived from the *S*-matrix theory [52]. From formula (7), moreover, the one- and two-photon ionization cross sections can be readily obtained by either setting $F^{(\omega)}$ or $F^{(2\omega)}$ to *zero*, and by normalizing on the incoming flux; cf reference [53]. Whereas the term of a two-photon cross section (in cm^4 s) might be slightly misleading at the first glance, it has been widely used in the literature of multi-photon processes and shows, that the absorption of two photons by a single atom is proportional to the square of the incoming photon flux.

In perturbation theory, the one- and two-photon angle-differential cross sections are given by

$$\frac{\mathrm{d}\sigma^{(2\omega)}}{\mathrm{d}\Omega}(\vartheta, \varphi; \epsilon^{(2\omega)}, \omega; n, \ell) = \frac{2\pi^2\alpha}{\omega} \sum_m M^{(2\omega)*}(nlm) M^{(2\omega)}(nlm).$$

$$\frac{\mathrm{d}\sigma^{(\omega)}}{\mathrm{d}\Omega}(\vartheta, \varphi; \epsilon^{(\omega)}, \omega; n, \ell) = \frac{8\pi^3\alpha^2}{\omega^2} \sum_m M^{(\omega)*}(nlm) M^{(\omega)}(nlm).$$

For the ionization of a *ns* inner-shell electron, these angle-differential cross sections can be further simplified within the electric-dipole approximation to

$$\frac{\mathrm{d}\sigma^{(2\omega)}}{\mathrm{d}\Omega}(\vartheta,\varphi;\epsilon^{(2\omega)},\omega;n,\ell=0) = \frac{9\pi\alpha}{2\omega}\left\{|U_p|^2\sin^2\vartheta\left[1+P_l^{(2\omega)}\cos(2\varphi)\right]\right\} \tag{8}$$

$$\begin{aligned}\frac{\mathrm{d}\sigma^{(\omega)}}{\mathrm{d}\Omega}(\vartheta,\varphi;\epsilon^{(\omega)},\omega;n,\ell=0) = \frac{9\pi^2\alpha^2}{2\omega^2}\Big\{&2|U_s|^2P_1^{(\omega)}\\ &+|U_d|^2\Big[2P_1^{(\omega)}-6\sin^2\theta\Big(P_1^{(\omega)}+P_1^{(\omega)}\cos(2\phi)\Big)\\ &+\frac{9}{2}\sin^4\theta\Big(1+P_1^{(\omega)}\cos(2\phi)\Big)^2\Big]\\ &+2\,\mathrm{Re}\Big[U_sU_d^*\,\mathrm{e}^{\mathrm{i}(\delta_s-\delta_d)}\Big[2P_1^{(\omega)}-3\sin^2\theta\Big(P_1^{(\omega)}[1+\cos(2\phi)]\\ &+iP_1^{(\omega)}P_c^{(\omega)}\sin(2\phi)\Big)\Big]\Big]\Big\},\end{aligned} \tag{9}$$

and where, for the sake of brevity, we made use of the short-hand notations $U_p \equiv U^{(E1)}\,(1s\to p)$ in equation (8), and $U_s \equiv U^{(E1,E1)}\,(1s\to p\to s)$ and $U_d \equiv U^{(E1,E1)}\,(1s\to p\to d)$ in equation (9), respectively. Moreover, $P_1^{(2\omega)}$, $P_1^{(\omega)}$ and $P_c^{(\omega)}$ refer to the degree of linear and circular polarization of the associated beam components.

With these expressions for the angle-differential cross sections and for the ionization of a *ns* inner-shell electron, and the biharmonic angle-differential rate (7) can be separated into three distinct contributions of different symmetry

$$\begin{aligned}&\frac{\mathrm{d}W^{(\omega,2\omega)}}{\mathrm{d}\Omega}(\vartheta,\varphi;\epsilon^{(\omega)},\epsilon^{(2\omega)};\Phi,F^{(\omega)},F^{(2\omega)};n,\ell=0)\\ &\qquad=\frac{\mathrm{d}W_{\mathrm{sym}}}{\mathrm{d}\Omega}(\epsilon^{(\omega)},\epsilon^{(2\omega)})+\frac{\mathrm{d}W_{\mathrm{dich}}}{\mathrm{d}\Omega}(\epsilon^{(\omega)},\epsilon^{(2\omega)})+\frac{\mathrm{d}W_{\mathrm{asym}}}{\mathrm{d}\Omega}(\epsilon^{(\omega)},\epsilon^{(2\omega)}),\end{aligned} \tag{10}$$

where the rate $\frac{\mathrm{d}W_{\mathrm{sym}}}{\mathrm{d}\Omega}$ in independent of the signs of $\epsilon^{(\omega)}$, $\epsilon^{(2\omega)}$ and, hence, always symmetric within the polarization planes, while $\frac{\mathrm{d}W_{\mathrm{dich}}}{\mathrm{d}\Omega}$ describes those contributions from the interplay of the one- and two-photon ionization amplitudes that results either in a one- or two-fold rotational symmetry. The third term $\frac{\mathrm{d}W_{\mathrm{asym}}}{\mathrm{d}\Omega}$, finally, refers to the up-down asymmetry due to the interference between the one- and two-photon ionization pathways. While we here display explicitly all the parametric dependencies on the left-hand side of equation (10), only the ellipticities $\epsilon^{(\omega)}$, $\epsilon^{(2\omega)}$ are shown for the individual terms as we shall focus on the polarization in the next section. However, the quite large number of (input) parameters in equation (10) makes it clear already why the biharmonic ionization enables one to steer the angular distributions of the emitted electrons to rather unparalleled shapes, and as we shall further detail in section 3 below. Appendix provides expressions for the three contributions in equation (10) to the biharmonic ionization rate of *ns* inner-shell electrons. Below, we shall show a number of typical photoelectron angular distributions following either an one-photon, nonresonant two-photon, or the biharmonic $(\omega, 2\omega)$ ionization of a 1*s* inner-shell electron from a neon target. These distributions exhibit different symmetries due to the interaction with the various beam components. In particular, we shall explain and discuss how these distributions explicitly depend on the polarization of the ionizing light.

For an unpolarized target, finally, the angle-differential one- and two-photon cross section just depends on the photon energy ω and the polar angle ϑ but are generally independent of the azimuthal angle φ. From the angle-differential ionization cross sections, moreover, the total cross sections can then be readily obtained by

$$\sigma(\epsilon,\omega) = \int \mathrm{d}\Omega\,\frac{\mathrm{d}\sigma(\vartheta,\varphi;\epsilon,\omega)}{\mathrm{d}\Omega}. \tag{11}$$

2.4. Dichroism signals

Apart from measuring the total ion yield or the photoelectron angular distribution, a dichroism in the light–matter interaction often reveals complementary information about its polarization or phase dependence. The circular dichroism of atoms and molecules, for example, probes the light–matter interaction for its asymmetry with regard to flipping the polarization of the incident light from a left-to right-polarized beam or, vice versa. A number of different (circular) dichroism signals can therefore be analyzed for the two-photon ionization of atoms and ions, if the incident beam carries in addition also an orbital angular momentum [55–57]. Other well-known dichroism signals in atomic or molecular physics refer to changing the orientiation of a magnetic field [58] or the chirality of molecules [59]. By using

polarized targets, moreover, the circular dichroism has been utilized in order to control the energy transfer in multi-photon ionization [60] or to analyze the intensity of the ionizing beam [10].

For atoms, a *non-zero* circular dichroism in the light–matter interaction can only arise if the target atoms are initially polarized. For monochromatic light, this rule applies quite general and independent of the number of absorbed photons. Unlike the circular dichroism, however, an ed does not require a prior polarization of the target. Instead, a (non-zero) ed signal can occur already within the single active-electron approximation, and without that any spin–orbit interaction has to be taken into account. Here, the ed is defined in terms of the angle-differential cross sections as

$$\Delta^{(\mathrm{ed})}(\vartheta,\varphi;\epsilon) = \left.\frac{\mathrm{d}\sigma(\epsilon) - \mathrm{d}(-\epsilon)}{\mathrm{d}\sigma(\epsilon) + \mathrm{d}(-\epsilon)}\right|_{\vartheta,\varphi}, \tag{12}$$

and where we use the notation $\mathrm{d}\sigma(\epsilon) \equiv \frac{\mathrm{d}\sigma}{\mathrm{d}\Omega}(\vartheta,\varphi;\epsilon)$. For a single beam, the ed therefore just expresses the normalized difference between the cross sections for an ionization of the target atoms as obtained by left- and right-elliptically polarized light.

We can use expression (12) to make the ed explicit for the 1*s* photoionization within the electric-dipole approximation. In the one-photon ionization, the electron just follows the $s \to p$ pathway and leaves the photoion with kinetic energy ε into direction (ϑ,φ). This is completely independent of the polarization and gives rise to $\Delta^{(\mathrm{ed}:2\omega)}\ (\vartheta,\varphi;\ \epsilon) = 0$. For the two-photon ionization, in contrast, the 1*s* electron can follow either a $s \to p \to s$ or $s \to p \to d$ pathway, and this leads to the ed

$$\begin{aligned}\Delta^{(\mathrm{ed}:\omega)}&(\vartheta,\varphi;\epsilon^{(\omega)};F^{(\omega)};n,\ell=0)\\ &= \frac{108(F^{(\omega)})^2\pi^2\alpha^2\omega^{-2}\,\mathrm{Re}\left[iU_sU_d^*\,\mathrm{e}^{\mathrm{i}(\delta_s-\delta_d)}P_c^{(\omega)}P_1^{(\omega)}\sin^2\vartheta\,\sin(2\varphi)\right]}{\frac{\mathrm{d}\sigma^{(\omega)}}{\mathrm{d}\Omega}(\vartheta,\varphi;\epsilon^{(\omega)};n,\ell=0) + \frac{\mathrm{d}\sigma^{(\omega)}}{\mathrm{d}\Omega}(\vartheta,\varphi;-\epsilon^{(\omega)};n,\ell=0)},\end{aligned} \tag{13}$$

and where the denominator just refers to the sum of the angle-differential cross sections for left- and right-elliptically polarized light. This normalization is the reason also that the flux $F^{(\omega)}$ appears explicitly in the expression, if we wish to write the nominator in terms of the radial amplitudes U_s, U_d as well as the degrees of linear and circular polarization of the incident light.

Finally, we can exploit the symmetries of the individual contributions in equation (10) to write the ed for the biharmonic ionization as

$$\begin{aligned}\Delta^{(\mathrm{ed}:\omega,2\omega)}&(\vartheta,\varphi;\epsilon^{(\omega)},\epsilon^{(2\omega)};\ldots;n,\ell=0)\\ &= \frac{\frac{\mathrm{d}W_{\mathrm{dich}}}{\mathrm{d}\Omega}(\epsilon^{(\omega)},\epsilon^{(2\omega)}) - \frac{\mathrm{d}W_{\mathrm{dich}}}{\mathrm{d}\Omega}(-\epsilon^{(\omega)},-\epsilon^{(2\omega)})}{\frac{\mathrm{d}W}{\mathrm{d}\Omega}(\vartheta,\varphi;\epsilon^{(\omega)},\epsilon^{(2\omega)}) + \frac{\mathrm{d}W}{\mathrm{d}\Omega}(\vartheta,\varphi;-\epsilon^{(\omega)},-\epsilon^{(2\omega)})}\end{aligned} \tag{14}$$

and which, quite obviously, depends also on $F^{(\omega)}$, $F^{(2\omega)}$ and Φ, i.e. the intensity and relative phase of the two beam components.

2.5. Computations

Any numerical analysis of the biharmonic $(\omega, 2\omega)$ ionization requires a fast and reliable access to the one- and two-photon amplitudes from sections 2.2 and 2.3. In particular, the two-photon amplitude (6) includes an infinite summation over the full (electron) *spectrum* whose evaluation remains a challenge for all perturbation calculations of many-electron atoms and ions beyond the first-order perturbation theory. Such a summation over the complete spectrum is however feasible in the single active-electron approximation, and if the detailed coupling of the photoelectron to the ionic core is neglected apart, from the (atomic) central-field potential of the photoion.

In the present work, all one- and two-photon amplitudes were calculated by means of a one-particle spectrum as obtained from Dirac's equation, and which thus includes also relativistic and spin–orbit contributions. For light and medium elements, however, relativistic contributions to the one- and two-photon amplitudes (5) and (6) are generally small but increase with the nuclear charge *Z*. Below, we therefore restrict our discussion to a nonrelativistic notation that also omits the coupling of the electron spin. This approximation applies to all elements, and especially as long as the $2p_{1/2} - 2p_{3/2}$ fine-structure is not resolved experimentally. Furthermore, we have applied a B-spline basis that reduces the infinite summation over the complete (one-electron) spectrum to a finite sum over a pseudo-spectrum, and where the (mean) interelectronic interaction with the other bound electrons is taken into account by a core-Hartree potential, cf reference [61]. This potential reproduces the 1*s* binding energy of atomic neon within $\pm 0.2\%$, when compared with experiment. For this pseudo-spectrum, moreover, we also analyzed the

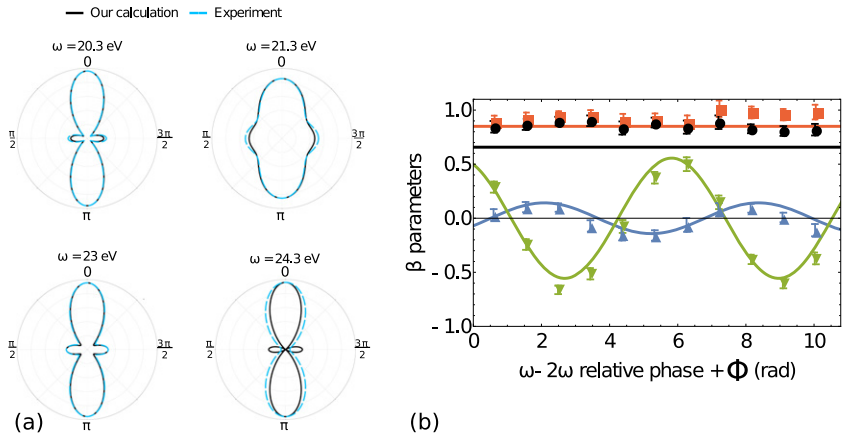

Figure 3. Photoelectron angular distribution and β_2 asymmetry parameters for the two-photon ionization of helium 1*s* electrons by linearly-polarized light. (a) Comparison of our computations (black solid line) in the single active-electron approximation with the measurements (blue dashed line) by Ma and co-workers [54] for four selected photon energies, $\hbar\omega = 20.3, 21.3, 23.0$ and 24.3 eV. (b) Comparison of β_2 asymmetry parameters for the biharmonic $(\omega, 2\omega)$ ionization of neutral helium by linearly-polarized light from this work (solid lines) and measurements (symbols) at $\hbar\omega = 14.3$ eV, as taken from reference [30].

summation over the magnetic-dipole ($M1$) and electric-quadrupole ($E2$) components of the radiation field but found them negligible for the present discussion [35].

Finally, to test our implementation of the amplitudes (5) and (6) and to critically evaluate the use of the single active-electron approximation, we calculated the photoelectron angular distributions for the two-photon as well as the biharmonic $(\omega, 2\omega)$ ionization of neutral helium by linearly-polarized light. For these ionization processes, several measurements [30, 54] are available from the literature. For example, figure 3(a) compares the photoelectron angular distributions for the two-photon ionization of helium at the photon energies $\hbar\omega = 20.3, 21.3, 23.0$ and 24.3 eV with the measurements by Ma and co-workers [54]. The good agreement with these experiments suggests that the transition amplitudes and phases are indeed well reproduced by our single active-electron treatment. Similarly, figure 3(b) compares the computed asymmetry parameters β_2 with the measurements of the biharmonic $(\omega, 2\omega)$ ionization by Di Fraia and co-workers [30] and confirms a quite reasonable agreement.

3. Discussion

3.1. Energy-dependent photoelectron emission. Resonances in the total cross sections

The two-photon inner-shell ionization of atoms has three *distinct* signatures which can be utilized to uniquely detect and analyze this nonlinear process. These signatures refer to (i) the well-defined energies $\varepsilon \approx \hbar\omega_1 + \hbar\omega_2 - \varepsilon_b$ of the emitted photoelectrons, (ii) the observation of fluorescence radiation owing to the subsequent filling of the inner-shell vacancy and (iii) the resonance behavior in the total cross sections as well as in most of the related—electron or photon—distributions, if the photon energy becomes resonant with any allowed inner-shell excitation of the atom. This resonance behavior (iii) covers even the initially occupied shells, such as the $1s \to 2p$ excitation of atomic neon owing to the quantum-mechanical time-order. Moreover, further signatures for a two-photon ionization may arise (iv) from the autoionization of the inner-shell hole states that often dominates over the fluorescence emission (ii), although such a secondary electron emission is much harder to detect in most multi-photon ionization experiments. All these signatures have been analyzed for selected atoms but often remain difficult to be resolved in good detail, since the two-photon signals need first to be separated from the competing one-photon ionization of other (sub-) valence shells.

Figure 4 displays the total one- and two-photon ionization cross sections along with the biharmonic $(\omega, 2\omega)$ rate for the ionization of neon 1*s* electrons by elliptically-polarized light as function of the incident (2ω) total photon energy. While the one-photon ionization cross section in figure 4(a) smoothly decreases $\sim (2\omega)^{-7/2}$ with the incident photon energy, the (b) two-photon cross section appears more sensitive as function of the photon energy. In this ionization, and by following Fano's propensity rule [62], the pathway with the highest orbital angular momentum typically dominates over the other pathways for initially unpolarized atoms. This rule generally applies also to the two-photon ionization of 1*s* electrons and gives then rise to mainly *d*-wave electrons; this dominance is however *reversed* near to the ionization threshold, where the $s \to p \to s$ pathway becomes largest. For low photon energies, moreover, the screening

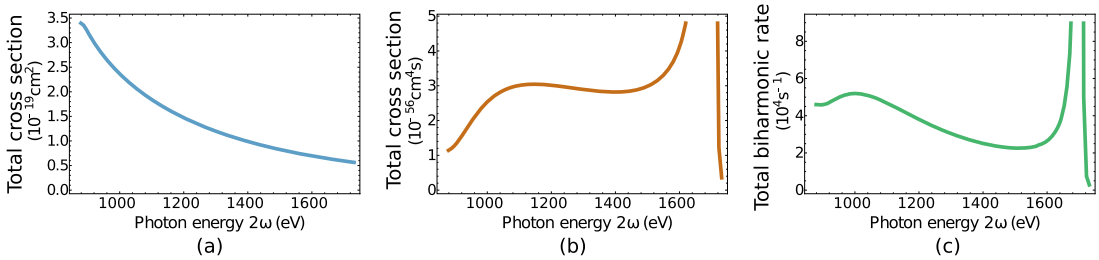

Figure 4. Total one-photon and two-photon cross section as well as total biharmonic (ionization) rate for the ionization of neon 1*s* electrons by elliptically-polarized light as function of the incident (2ω) photon energy. While (a) the one-photon ionization cross section smoothly decreases $\sim (2\omega)^{-7/2}$ with the incident photon energy, the (b) two-photon cross section depends more sensitive on the incoming photon energy. At low (2ω) photon energies, this two-photon cross section is for neon rather small due to the screening by the other electrons, while it becomes resonantly enhanced at $\hbar\omega \approx 825$ eV because of the possible $1s \to 2p$ excitation. The total $(\omega, 2\omega)$ biharmonic ionization rate is then the sum of the one-photon and two-photon cross sections, each multiplied with the associated flux $F^{(2\omega)} = 10^{14}$ W cm^{-2} and $F^{(\omega)} = 4 \times 10^{9}$ W cm^{-2}, respectively.

of the photoelectron by the $2s + 2p$ electron density reduces the two-photon ionization cross section [51], while it becomes resonantly enhanced at $\omega \approx 825$ eV owing to the $1s \to 2p$ inner-shell excitation. No interference occurs for the total biharmonic $(\omega, 2\omega)$ ionization rate because of the orthogonality of the spherical harmonics, as they are associated with the one-photon $s \to p$ as well as the two-photon $s \to p \to s$ or $s \to p \to s$ ionization pathways. This behavior is quite in contrast to general biharmonic $(m\omega, n\omega)$ ionization processes with $m + n =$ even, which show rather distinct interference features.

3.2. Characteristic angular distributions following the ionization by elliptical light

To better understand the angle-dependent biharmonic $(\omega, 2\omega)$ ionization yield, let us first consider the one- and two-photon ionization of atoms separately. Figure 5 displays characteristic photoelectron angular distributions following the ionization of a 1*s* electron by linearly-, circularly- and elliptically-polarized light. For linearly-polarized light, for example, the angular distribution from the one- and two-photon ionization are always rotationally symmetric with regard to the polarization vector (*x*-axis) and obey a mirror symmetry with regard to the *y*–*z* plane, perpendicular to this vector. Quite analog symmetries also apply for circularly-polarized light but then with regard to the propagation direction (*z*-axis) of the incident light as well as the *x*–*y* polarization plane. All these symmetries are readily understood by the (projected) spin-angular momentum of the outgoing photoelectron. For the two-photon ionization by circularly-polarized light ($P_c = 1$), for instance, only the partial *d* waves with $m = \pm 2$ contribute to the photoelectron angular distributions and, hence, ensures again these symmetries. For elliptically-polarized light, however, only the one-photon angular distribution still follows the expected 'dipole' coils (cf figure 5(c)), while the two-photon distribution has no global symmetry anymore. In fact, these distributions apply for the ionization of any *ns* (inner-shell) electrons, a behavior that is readily deduced also from the $s \to p$ one-photon as well as the $s \to p \to s$ and $s \to p \to s$ two-photon pathways, since the angular distribution of each pathway is determined by the orbital angular momentum partial waves of the outgoing photoelectron or, speaking more technically, by the shape of the associated spherical harmonics.

For the biharmonic $(\omega, 2\omega)$ ionization, in contrast, quite different and asymmetric photoelectron angular distributions occur that cannot appear in any multi-photon ionization by monochromatic light alone. For linearly-polarized light, for example, an up-down asymmetry occurs with regard the *y*–*z* plane, although the angular distribution remains itself rotationally symmetric around the polarization vector. This asymmetry arises from the interference of the one- and two-photon ionization pathways, and its shape can be readily controlled by the phase Φ between the two beam components. The rotational symmetry of the angular distribution is broken also for circularly-polarized light, and this applies to both, a co- and counter-rotating circular polarization of the two beam components. Still, a symmetric three-lobe distribution occurs for the biharmonic ionization with counter-rotating circularly-polarized beams, in line with the counter-rotation of the electric-field vector of all bicircular beams [27]. For elliptically-polarized light, finally, both the rotational and all mirror symmetries are generally broken, making the angular distributions particularly sensitive with regard to the electronic structure of the target atoms as well as to the polarization properties of the incident light. Although such simple symmetries may help describe the photoelectron distributions in multi-photon ionization measurements of inner-shell electrons, in practice quite significant deviations may occur owing to the screening by other electrons as well as to the fine-structure, i.e. relativistic contributions, to the transition amplitudes.

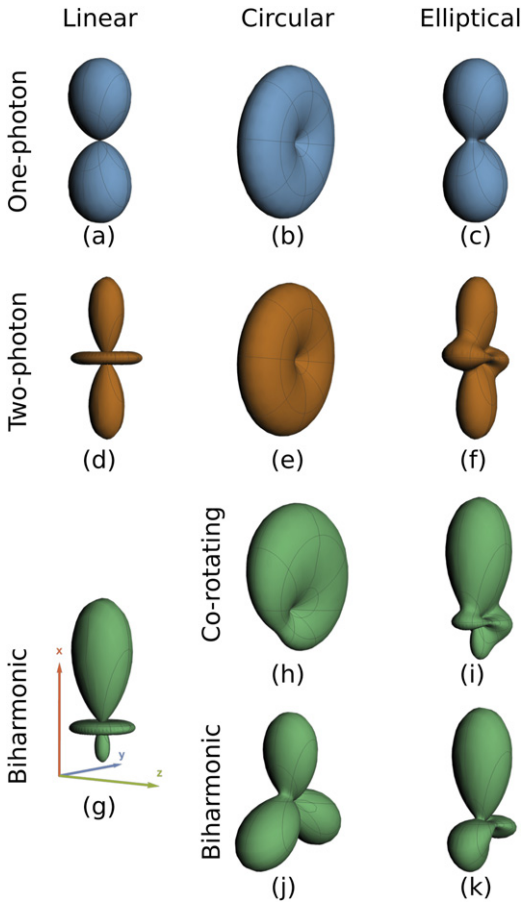

Figure 5. Typical photoelectron angular distributions following the one-photon (a)–(c), nonresonant two-photon (d)–(f) and biharmonic $(\omega, 2\omega)$ ionization (g)–(k) of neutral closed-shell atoms by incident light of different polarization. In particular, the biharmonic ionization generally introduces an asymmetry in the photoelectron angular distributions that does not appear in any multi-photon ionization by monochromatic light. See text for further discussion of these angular distributions.

3.3. Circular dichroism in biharmonic ionization

A circular dichroism arises from the asymmetric interaction of the atoms with the radiation field, if light of different handeness, i.e. left-versus right-circularly polarized light, is applied. No such dichroism is however possible for the one- or two-photon ionization of initially unpolarized atoms, since there is only a single ionization pathway, either $s \to p$ or $s \to p \to d$, for circularly-polarized incident radiation. This is easily seen also from the spin-angular momentum of the outgoing photoelectron or the vanishing φ-dependence, $e^{im\varphi *} \cdot e^{im\varphi} = 1$ in the square of the associated transition amplitude. As seen from figure 6, a constant photoelectron angular distribution in the polarization plane occurs for the one- and two-photon ionization with circularly-polarized light, independent of its handedness, and which leads to a *zero* dichroism $\Delta^{(cd)} = 0$ in both cases.

For the biharmonic $(\omega, 2\omega)$ ionization of *ns* inner-shell electrons, however, a circular dichroism may occur in the photoelectron angular distribution already for the ionization of unpolarized atoms owing to the interference between the one- and two-photon ionization pathways. Figure 6(c) displays the angular distributions for biharmonic ionization of neon 1*s* electrons and a counter-rotating $(\omega, 2\omega)$ beam. For such a beam, the circular dichroism can always be maximized by just tuning the phase difference Φ as well as the relative intensities of the $(\omega, 2\omega)$ beam components. This is readily seen also from figure 7 that demonstrates how the photoelectron angular distribution and, hence, the circular dichroism (shown by the color-coded ring around the distributions) can be steered in the biharmonic $(\omega, 2\omega)$ ionization of neon 1*s* electrons. Photoelectron distributions are displayed for the ionization by a $(↺, \omega)$ and $(↻, 2\omega)$ beam (dashed light-green line) as well as for a $(↻, \omega)$ and $(↺, 2\omega)$ beam (solid dark line). In general, a left-right flip of both elliptically-polarized beam components result in a nonzero overlap of the photoelectron distributions and, thus, a circular dichroism for most choices of parameters. This overlap of the two distributions in figure 7(a) can be modified by either changing the intensity in figure 7(b) or the phase Φ in figure 7(c) between the beam components. As seen from figure 7(d), moreover, it is always possible to tune

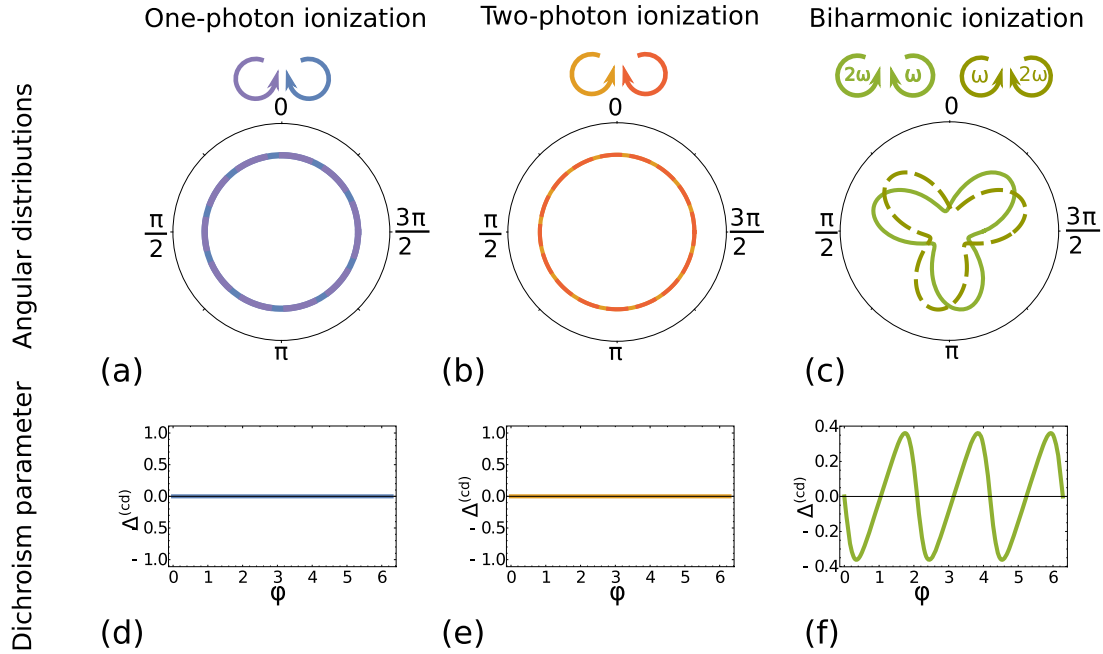

Figure 6. Angular distribution (a)–(c) and circular dichroism (d)–(f) in the one-photon (left), two-photon (middle) and biharmonic $(\omega, 2\omega)$ ionization (right) of neon 1*s* electrons. Since the photoelectron angular distribution does not depend on the handedness of the circular polarization for the one- and two-photon ionization of unpolarized atoms, the circular dichroism, $\Delta^{(\mathrm{cd})}(\vartheta, \varphi) = 0$, must vanish identically. For the biharmonic $(\omega, 2\omega)$ ionization, however, the circular dichroism $\Delta^{(\mathrm{cd})}(\vartheta, \varphi)$ is non-zero because of the interference between the $s \to p$ one-photon as well as the $s \to p \to s$ and $s \to p \to d$ two-photon pathways. This asymmetry is seen also from the total electric field of the two biharmonic beam components.

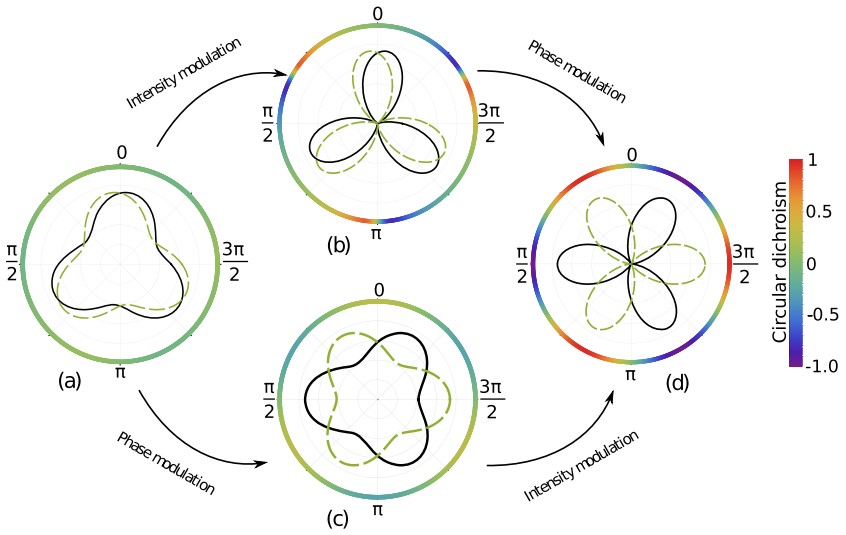

Figure 7. Steering the photoelectron angular distributions, and hence the circular dichroism $\Delta^{(\mathrm{cd})}(\vartheta, \varphi)$ (shown by the color-coded ring around the distributions) in the biharmonic $(\omega, 2\omega)$ ionization of neon 1*s* electrons. Photoelectron distributions are shown for the ionization by a $(\circlearrowleft, \omega)$ and $(\circlearrowright, 2\omega)$ beam (dashed light-green line) as well as for $(\circlearrowright, \omega)$ and $(\circlearrowleft, 2\omega)$ beam (solid dark line). (a) Both distributions generally exhibit an overlap and, hence, a circular dichroism for most choices of parameters. This overlap of the two distributions can be modified by either changing the intensity (b) or the phase Φ (c) between the beam components. A maximum value of the circular dichroism $\Delta^{(\mathrm{cd})} = \pm 1$ (d) is obtained if both, the intensity and/or phase, are properly adjusted.

the circular dichroism to its maximum $\Delta^{(\mathrm{cd})} = \pm 1$ as well as to $\Delta^{(\mathrm{cd})} = 0$, and which help analyze the polarization purity of the ionizing beam.

3.4. Elliptical dichroism in two-photon and biharmonic $(\omega, 2\omega)$ ionization

Like for circularly-polarized light, the ed in the photoelectron angular distribution just characterizes the left-right asymmetry, if atoms interact with left- and right-handed elliptically-polarized light. Indeed, quite

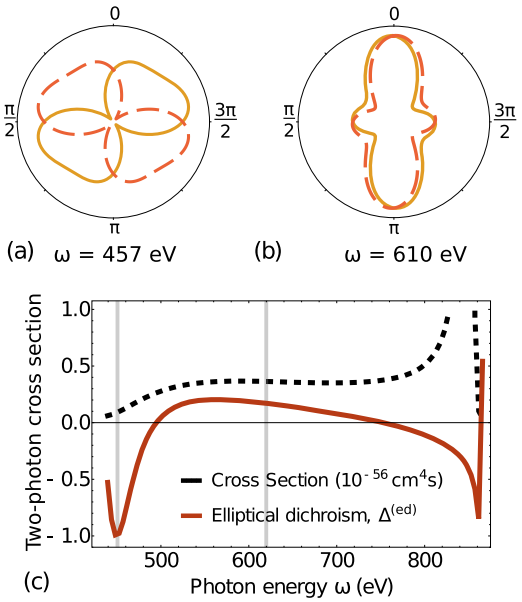

Figure 8. Two-photon ionization of neon 1*s* electrons by elliptically-polarized light with ellipticity $\epsilon = 0.42$. (a) and (b) Photoelectron angular distributions for the ionization by left-handed (dashed red line) and right-handed (solid orange line) elliptically-polarized beams. While these distributions clearly differ from each other at low energies $\hbar\omega = 457$ eV due to the screening by the other bound electrons (a), they nearly overlap at high photon energy $\hbar\omega = 610$ eV in line with a weak ed. (c) The ed (red solid line) as function of the incident photon energy, and together with the total two-photon ionization cross section in units of 10^{-56} cm^4 s. The energies of the distributions (a) and (b) are marked by gray vertical lines; see text for further discussion.

complex photoelectron angular distribution arise in the biharmonic $(\omega, 2\omega)$ ionization of unpolarized atoms with elliptically-polarized light if the circular polarization is simultaneously flipped for both $(\omega, 2\omega)$ beam components. A flip of the handedness of just one component is of less interest as it results in very different electric fields and, hence, angular distributions that are hardly related to each other. If both circular components are flipped together, however, the overall shape of the electric field remains the same, though the electric field vector now rotates in opposite direction.

Let us begin our discussion with the two-photon ionization of neon 1s electrons by elliptically polarized light, as discussed in section 2.4, an ed may arise from the (single) interference term (13) due to the interplay of the $s \to p \to s$ and $s \to p \to d$ pathways. For the ionization of neon 1*s* electrons, figures 8(a) and (b) displays the photoelectron angular distributions for the ionization by left-handed (dashed red line) and right-handed (solid orange line) elliptically-polarized light. While these distributions clearly differ from each other at low energies $\hbar\omega = 457$ eV due to the screening by the other bound electrons (figure 8(a)), they nearly overlap at high photon energy $\hbar\omega = 610$ eV (figure 8(b)), and as seen by the weak ed. Moreover, figure 8(c) shows the total two-photon ionization cross section for elliptically-polarized light with ellipticity $\epsilon = 0.42$ (black dashed line), and together with the ed (red solid line) as function of the incident photon energy.

For the biharmonic $(\omega, 2\omega)$ ionization with elliptical light, the interference of the one-photon (2ω) and two-photon (ω) beam components is crucial in order to analyze and understand the angular distributions. Instead of just a single interference term, as discussed above for the two-photon ionization alone, additional terms here arise from the interference of the one- and two-photon ionization pathways. This is demonstrated in figure 9, which compares the symmetry in the photoelectron angular distribution (upper raw), the ed (middle raw) and well as for selected contributions (lower raw) to the one- and two-photon as well as biharmonic ionization. All these distributions are shown in the x–y polarization plane of the incident light field and are computed for neon 1*s* electrons and an ellipticity $|\epsilon| = 0.42$. While the angular distribution (angle-differential cross sections) are always positive, the different contributions in the lower raw of figure 9 display different mirror symmetries and can be both, positive and negative.

Especially the ed in figure 9(f) shows a rich structure with local minima and maxima, and which can be readily understood in terms of the $s \to p \to s$ and $s \to p \to d$ ionization pathways. The ed is always zero, $\Delta^{(\mathrm{ed})}(\vartheta, \varphi) = 0$, whenever at least one of the pathways has a zero amplitude, while it becomes ± 1 if the ratio of the (radial) amplitudes reaches its optimal value $U^{(E1,E1)}(1s \to p \to d)/U^{(E1,E1)}(1s \to p \to s) = 1/\sqrt{2}$. In general, however, it appears quite difficult to predict in advance the sign and magnitude of the dichroism $\Delta^{(\mathrm{ed}:\omega,2\omega)}(\vartheta, \varphi;\ \epsilon^{(\omega)}, \epsilon^{(2\omega)};\ \ldots;\ n, \ell = 0)$ as function of

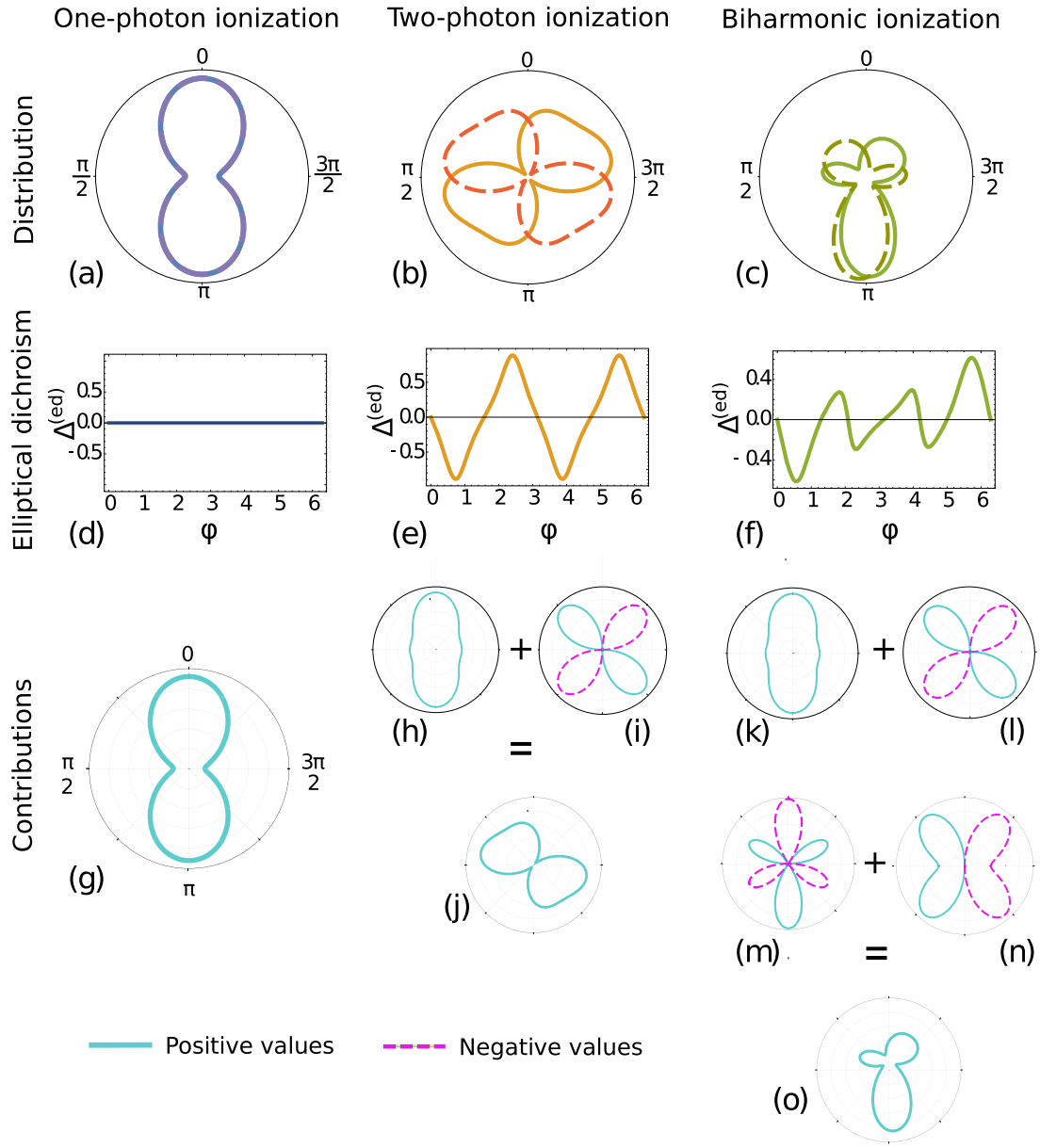

Figure 9. Comparison of symmetries in the photoelectron angular distribution (upper raw), the ed (middle raw) and well as for selected contributions (lower raw) to the one- and two-photon as well as biharmonic ionization. All these distributions are shown in the x–y polarization plane of the incident light field and are computed for neon 1s electrons and an ellipticity $|\epsilon| = 0.42$. While the angular distribution (angle-differential cross sections) are always positive, the different contributions in the lower raw can be distinguished due to their mirror symmetries and can be both, positive (solid turquoise linea) and negative (dashed pink linea). See text for further discussion.

the ellipticities of the two beam components as well as their relative phase Φ. This particularly applies near to the two-photon ionization threshold where detailed calculations are needed in order to account for the screening by the other bound electrons.

One can decompose the angle-differential cross section for the biharmonic $(\omega, 2\omega)$ ionization into a symmetric and antisymmetric contribution as shown in section 2.3. The lower raw of figure 9 disposes various of the contributions to the angle-differential cross section within the x–y polarization plane. For instance, the symmetric contribution in figure 9(h) refers to the squared terms in the radial amplitudes $|U_{s,d}|^2$ from equation (9), together with the symmetric part from the interference term. Similarly, the dichroic contribution in figure 9(i) refers to the last term of equation (9), and which is the only one that depends on the photon handedness. The sign of the ellipticity $\epsilon^{(\omega)}$ and the phase difference $\delta_s - \delta_d$ here determine the intervals, for which dichroic term $\frac{dW_{\rm dich}}{d\Omega}$ contributes constructively (turquoise) or destructively (pink) to the angular distribution. The sum of the symmetric and the dichroic contributions finally gives rise to the final photoelectron angular distribution in figure 9(j). The relative contributions of the symmetric and dichroic parts, and hence the magnitude of the left-right asymmetry, are hereby determined again by the ratio of the partial waves $U^{(E1,E1)}$ $(1s \to p \to d)/U^{(E1,E1)}$ $(1s \to p \to s)$.

A similar analysis can be made for the left-right asymmetry of the one- and two-photon ionization pathways. For example, the interference between the $s \to p \to s$ and $s \to p \to d$ ionization pathways leads to a 'cross-type' structure in figure 9(l), i.e. the change of sign under either a x or y mirror transformation. This antisymmetry then also occurs for the biharmonic ionization. Another left-right symmetry arises from the interference of the one- and two-photon ionization pathways as shown in figure 9(n). This term reverses its sign only for a mirror transformation with regard to the x axis. Therefore, if treated separately, an up-down or left-right symmetry occurs for both, the one- and two-photon ionization of ns electrons by elliptically-polarized light, wherease these symmetries are generally broken for biharmonic ionization processes as finally seen from figure 9(o).

3.5. Biharmonic ($m\omega$, $n\omega$) multi-photon ionization by circularly-polarized light

For the multi-photon ionization of atoms and molecules, the complexity (in the shape) of the photoelectron angular distributions and associated dichroisms increases markedly with each additionally absorbed photon. This is perhaps most readily seen already from the length and number of the (multiple) ionization pathways that describe such multi-photon processes.

In the biharmonic $(m\omega, n\omega)$ ionization of atomic inner-shell electrons, we are interested especially into those photoelectrons that are released by the interplay of $n \times (m\omega) = m \times (n\omega)$ photons. For these photoelectrons, generally $m + n$ photons contribute to the angle-differential and total cross sections, and give rise to quite composite distributions. If $m + n$ is odd, the partial wave of the two pathways below

$$s \to \underbrace{\ell_1 \to \ell_2 \to \cdots \to \ell_n}_{n\times(m\omega)\text{photons}} \qquad \text{and} \qquad s \to \underbrace{\ell'_1 \to \ell'_2 \to \cdots \to \ell_m}_{m\times(n\omega)\text{photons}}$$

always have different parity ($\ell_n \neq \ell_m$) and, thus, will not interfere with each other in the total cross sections owing to the orthogonality of the spherical harmonics. However, they *do* interfere in the photoelectron angular distribution since all mixed terms $Y^*_{\ell_m m_m} Y_{\ell_n m_n}$ will appear in the bilinear product $M^{(\omega+2\omega)*} M^{(\omega+2\omega)}$. If $n + m$ is even, in contrast, some of the pathways always result into the same partial waves ($\ell_m = \ell_n$) of the emitted photoelectrons, and this alone already leads to interferences also in the total ionization cross section. For this $(m\omega, n\omega)$ ionization, moreover, one needs to flip again the circular polarization of both beam components simultaneously in order to observe a non-trivial dichroism signal. While, at present, the biharmonic $(m\omega, n\omega)$ ionization of inner-shell electrons is still an experimental challenge, such measurements may become more realistic for the ionization of $n's$ valence-shell electrons from alkali vapors by circularly- or elliptically-polarized light.

Following Fano's propensity rule [62], the wave function of the outgoing photoelectrons in all $(m\omega, n\omega)$ biharmonic ionization processes with circularly-polarized beams of helicity λ_m, λ_n will likely be dominated by just two (nonrelativistic) partial waves

$$\psi^{mn}_{\lambda_m \lambda_n}(\vartheta, \varphi) == c_{mn}(\lambda_n) Y_{m, \lambda_n \cdot m} + c_{nm}(\lambda_m) \mathrm{e}^{\mathrm{i}\Phi} Y_{n, \lambda_m \cdot n} \tag{15}$$

with the Fourier coefficients

$$c_{mn}(\lambda_n) = \frac{\sqrt{4\pi}(-2\lambda_n)^m\, m!}{(2m+1)!} \left(\frac{-9\pi\alpha F^{(n\omega)}}{m\omega} \right)^{m/2} \mathrm{e}^{\mathrm{i}\delta_m} U_m.$$

In this expression, δ_m refers to the phase of the ℓ_mth partial wave and $F^{(n\omega)} = E_n^2/(n\omega)$ to the flux of the associated beam component with the intensity $I^{(n\omega)} = n\omega F^{(n\omega)}$. Indeed, the expression (15) of the photoelectron wave function is formed analog to the bilinear product from above but can be analyzed more easily for its dominant contributions. If the photoelectron distribution is just given by the two spherical harmonics $Y_{\ell, \pm\ell}(\vartheta, \varphi)$ with $\ell = m, n$, the weight and sign of the contributions with the magnetic quantum numbers $\pm\ell$ are given by the weight and the helicity of the corresponding beam components. Apart from this very brief discussion here, further work will be needed in order to elaborate the $(m\omega, n\omega)$ biharmonic photoionization and to exploit its angular distribution for electron spectroscopy.

4. Summary and conclusions

The biharmonic $(\omega, 2\omega)$ inner-shell ionization of atoms by circularly- and elliptically-polarized light has been analyzed and illustrated in terms of the ion yields, photoelectron angular distributions as well as the circular dichroism or ed. While, for the one- and two-photon ionization of inner-shell electrons, most spectroscopic observations can readily be explained in terms of the dominant ionization pathways, the photoelectron spectra exhibit already a much richer structure for the biharmonic $(\omega, 2\omega)$ ionization, as perhaps the simplest case of a multi-photon, multi-color ionization process. Most of the predicted features

in these spectra arise from interferences of the one- and two-photon amplitudes and can be understood already within the single active-electron approximation, in which the coupling of the valence-shell electrons and other many-electron correlations are neglected. For the ionization of K-shell electrons with FEL radiation, however, this single active-electron approximation is certainly well suited. Moreover, all the discussion has been made throughout within the electric-dipole approximation; many further asymmetries in the angular distribution and dichroism will become visible if magnetic and higher-electric (than $E1$) multipole transitions contribute to the inner-shell ionization or if the Lorentz force become relevant for the incoming beam [63].

The biharmonic $(\omega, 2\omega)$ inner-shell ionization of $1s$ electrons refers especially to the interplay of the $s \to p$ one-photon pathway and the $s \to p \to s$ and $s \to p \to d$ two-photon ionization pathways. The interference between these pathways gives rise to a number of unexpected phenomena, such as a circular dichroism in the biharmonic ionization of unpolarized atoms, an ed for most targets or a pronounced up-down asymmetry in the angular distribution with regard to the polarization vector as quantization axis. For the biharmonic $(\omega, 2\omega)$ ionization, the interference of the one- and two-photon ionization pathways leads to asymmetries in the angular distribution (within the polarization plane) that can be further steered by the phase Φ between the two (biharmonic) beam components. This asymmetry in the angular distribution gives rise also to a rich structure in the ed with local minima and maxima which are associated with the ionization pathways but which require detailed computations of the radial amplitudes involved for any quantitative prediction.

Apart from the coupling of the radiation field and, hence, the selection of possible pathways of the biharmonic $(\omega, 2\omega)$ ionization, the photoelectron angular distribution in the biharmonic ionization is strongly affected also by the screening of the nuclear charge by the remaining electrons. Indeed, this screening alone may result already in a rather strong ed in the photoelectron angular distributions. This ed can be further enhanced by tuning either the phase Φ or the intensity (ratio) of the ω and 2ω beam components, and can then be utilized as a tool for analyzing the polarization of the incident FEL radiation.

Further theoretical work along these lines will help improve our understanding of the ed and chirality, in particular if the explicit shell structure of the atoms and ions is taken into account [64]. Beside of biharmonic $(m\omega, n\omega)$ ionization process, including the case of the $(\omega, 3\omega)$ ionization, a detailed modeling of multi-photon ionization processes might support phase-of-the-phase measurements [65] and, thus, help extract structural (or even dynamical) information with high accuracy. This also enables one to steer the light–matter interaction from the recent strong-field ionization studies [66, 67] toward lower intensities and/or longer wavelength, or to the use of twisted light [68] or ultra-fast pulses [69].

Acknowledgments

This work has been funded by the Deutsche Forschungsgemeinschaft (DFG, German Research Foundation)—440556973.

Data availability statement

All data that support the findings of this study are included within the article (and any supplementary files).

Appendix. Angle-differential biharmonic ionization rate

For the biharmonic ionization of ns inner-shell electrons, the angle-differential ionization rate (10) can be decomposed into three terms of different symmetry, and which are given by:

$$\begin{aligned}\frac{\mathrm{d}W_{\mathrm{sym}}}{\mathrm{d}\Omega}(\epsilon^{(\omega)}, \epsilon^{(2\omega)}) = {} & \frac{9\pi\alpha F^{(2\omega)}}{2\omega}\left\{|U_p|^2 \sin^2\vartheta\left[1 + P_1^{(2\omega)}\cos(2\varphi)\right]\right\} \\ & + \frac{36(F^{(\omega)})^2\pi^2\alpha^2}{\omega^2}\left\{|U_s|^2\left(P_1^{(\omega)}\right)^2\right. \\ & + |U_d|^2\left[\left(P_1^{(\omega)}\right)^2 - 3P_1^{(\omega)}\sin^2\vartheta\left(P_1^{(\omega)} + \cos(2\varphi)\right)\right. \\ & \left. + \frac{9}{4}\sin^4\vartheta\left(1 + P_1^{(\omega)}\cos(2\varphi)\right)^2\right] \\ & \left. + 2\,\mathrm{Re}\left[U_s U_d^* \mathrm{e}^{\mathrm{i}(\delta_s - \delta_d)} P_l^{(\omega)}\left(P_l^{(\omega)} - \frac{3}{2}\sin^2\vartheta\left[P_1^{(\omega)} + \cos(2\varphi)\right]\right)\right]\right\} \end{aligned} \tag{A.1}$$

$$\frac{\mathrm{d}W_{\mathrm{dich}}}{\mathrm{d}\Omega}(\epsilon^{(\omega)},\epsilon^{(2\omega)}) = \frac{108\left(F^{(\omega)}\right)^2\pi^2\alpha^2}{\omega^2}\mathrm{Re}\Big[iU_sU_d^*\,\mathrm{e}^{\mathrm{i}(\delta_s-\delta_d)}P_{\mathrm{c}}^{(\omega)}P_{\mathrm{l}}^{(\omega)}\sin^2\vartheta\,\sin(2\varphi)\Big]$$
$$+\frac{18(\pi\alpha)^{3/2}F^{(\omega)}\sqrt{F^{(2\omega)}}}{\sqrt{1+(\epsilon^{(2\omega)})^2}\omega^{3/2}}\Big\{2\,\mathrm{Re}\Big[U_pU_s^*\,\mathrm{e}^{\mathrm{i}(\delta_p-\delta_s)}\,\mathrm{e}^{\mathrm{i}\Phi}P_{\mathrm{l}}^{(\omega)}\epsilon^{(2\omega)}\,\sin(\vartheta)\,\sin\varphi\Big]$$
$$+\mathrm{Re}\Big[U_pU_d^*\,\mathrm{e}^{\mathrm{i}(\delta_p-\delta_d)}\,\mathrm{e}^{\mathrm{i}\Phi}\Big(2P_{\mathrm{l}}^{(\omega)}\epsilon^{(2\omega)}\,\sin\vartheta\,\sin\varphi$$
$$+3\sin^3\vartheta\Big[P_{\mathrm{c}}^{(\omega)}\,\cos\varphi\,\sin(2\varphi)-\epsilon^{(2\omega)}\,\sin\varphi\Big(P_{\mathrm{l}}^{(\omega)}-\cos(2\varphi)\Big)\Big]\Big)\Big]\Big\} \tag{A.2}$$

$$\frac{\mathrm{d}W_{\mathrm{asym}}}{\mathrm{d}\Omega}(\epsilon^{(\omega)},\epsilon^{(2\omega)}) = \frac{-18(\pi\alpha)^{3/2}F^{(\omega)}\sqrt{F^{(2\omega)}}}{\sqrt{1+(\epsilon^{(2\omega)})^2}\omega^{3/2}}\Big\{2\,\mathrm{Re}\Big[-iU_pU_s^*\,\mathrm{e}^{\mathrm{i}(\delta_p-\delta_s)}\,\mathrm{e}^{\mathrm{i}\Phi}P_{\mathrm{l}}^{(\omega)}\,\sin\vartheta\,\cos\varphi\Big]$$
$$+\mathrm{Re}\Big[iU_pU_d^*\mathrm{e}^{\mathrm{i}(\delta_p-\delta_d)}\,\mathrm{e}^{\mathrm{i}\Phi}\Big(-2P_{\mathrm{l}}^{(\omega)}\,\sin\vartheta\,\cos\varphi$$
$$+3\sin^3\vartheta\Big[\epsilon^{(2\omega)}P_{\mathrm{c}}^{(\omega)}\,\sin\varphi\,\sin(2\varphi)+\cos\varphi\Big(P_{\mathrm{l}}^{(\omega)}+\cos(2\varphi)\Big)\Big]\Big)\Big]\Big\} \tag{A.3}$$

and where, for the sake of convenience, we made use of the short-hand notations $U_p \equiv U^{(E1)}(1s \to p)$ and $U_s \equiv U^{(E1,E1)}(1s \to p \to s)$ and $U_d \equiv U^{(E1,E1)}(1s \to p \to d)$, respectively. Moreover, $P_{\mathrm{l}}^{(2\omega)}$, $P_{\mathrm{l}}^{(\omega)}$ and $P_{\mathrm{c}}^{(\omega)}$ here refer to the degree of linear and circular polarization of the associated beam components.

ORCID iDs

S Fritzsche https://orcid.org/0000-0003-3101-2824
J Hofbrucker https://orcid.org/0000-0002-5917-3649

References

[1] Zernik W 1964 *Phys. Rev.* **135** A51
[2] Koval P, Fritzsche S and Surzhykov A 2003 *J. Phys. B: At. Mol. Opt. Phys.* **37** 375
[3] Surzhykov A *et al* 2011 *Phys. Rev.* A **84** 022511
[4] Ghimire S *et al* 2016 *Phys. Rev.* A **94** 043418
[5] Tamasaku K *et al* 2014 *Nat. Phys.* **8** 313
[6] Tamasaku K *et al* 2018 *Phys. Rev. Lett.* **121** 083901
[7] Richardson V *et al* 2010 *Phys. Rev. Lett.* **105** 013001
[8] Szlachetko J *et al* 2016 *Sci. Rep.* **6** 33292
[9] Tyrala K *et al* 2019 *Phys. Rev.* A **99** 052509
[10] Ilchen M *et al* 2017 *Phys. Rev. Lett.* **118** 013002
[11] Grum-Grzhimailo A N, Douguet N, Meyer M and Bartschat K 2019 *Phys. Rev.* A **100** 033404
[12] Young L *et al* 2010 *Nature* **466** 56
[13] Meyer M *et al* 2010 *Phys. Rev. Lett.* **104** 213001
[14] Schmiegelow C, Schulz J, Kaufmann H, Ruster T, Poschinger U G and Schmidt-Kaler F 2016 *Nat. Commun.* **7** 12998
[15] De Ninno G *et al* 2020 *Nat. Photon.* **14** 554
[16] Matula O, Hayrapetyan A G, Serbo V G, Surzhykov A and Fritzsche S 2013 *J. Phys. B: At. Mol. Opt. Phys.* **46** 205002
[17] Surzhykov A, Seipt D and Fritzsche S 2016 *Phys. Rev.* A **94** 033420
[18] Verhoef A J, Mitrofanov A V, Nguyen X T, Krikunova M, Fritzsche S, Kabachnik N M, Drescher M and Baltuška A 2011 *Laser Phys.* **21** 1270
[19] Callegari C *et al* 2021 *Phys. Rep.* **904** 1
[20] Fritzsche S, Grum-Grzhimailo A N, Gryzlova E V and Kabachnik N M 2008 *J. Phys. B: At. Mol. Opt. Phys.* **41** 165601
[21] Fritzsche S, Grum-Grzhimailo A N, Gryzlova E V and Kabachnik N M 2011 *J. Phys. B: At. Mol. Opt. Phys.* **44** 175602
[22] Mondal S *et al* 2013 *J. Phys. B: At. Mol. Opt. Phys.* **46** 164022
[23] Varvarezos L *et al* 2021 *Phys. Rev.* A **103** 022832
[24] Pengel D *et al* 2017 *Phys. Rev. Lett.* **118** 053003
[25] Armstrong G S J *et al* 2019 *Phys. Rev.* A **100** 063416
[26] Milosevic D B, Becker W and Kopold R 2000 *Phys. Rev.* A **61** 063403
[27] Paufler W, Böning B and Fritzsche S 2018 *Phys. Rev.* A **98** 011401(R)
[28] Paufler W, Böning B and Fritzsche S 2019 *J. Opt.* **21** 094001
[29] Prince K C *et al* 2016 *Nat. Photon.* **10** 176
[30] Di Fraia M *et al* 2019 *Phys. Rev. Lett.* **123** 213904
[31] Mazza T *et al* 2020 *Phys. Rev.* X **10** 041056
[32] Bashkansky M, Bucksbaum P H and Schumacher D W 1988 *Phys. Rev. Lett.* **60** 2458
[33] Florescu V, Budriga O and Bachau H 2011 *Phys. Rev.* A **84** 033425
[34] Gazibegovic-Busuladzic A, Becker W and Milosevic D B 2018 *Opt. Express* **26** 12684
[35] Hofbrucker J, Volotka A V and Fritzsche S 2018 *Phys. Rev. Lett.* **121** 053401
[36] Mousavi S A, Plum E, Shi J and Zheludev N I 2015 *Sci. Rep.* **5** 8977

[37] Khanikaev A B *et al* 2016 *Nat. Commun.* **7** 12045
[38] Paulus G G, Zacher F, Walther H, Lohr A, Becker W and Kleber M 1998 *Phys. Rev. Lett.* **80** 484
[39] Böning B, Paufler W and Fritzsche S 2018 *Phys. Rev.* A **98** 023407
[40] Beaulieu S *et al* 2000 *Nat. Phys.* **14** 484
[41] Douguet N, Grum-Grzhimailo A N, Gryzlova E V, Staroselskaya E I, Venzke J and Bartschat K 2016 *Phys. Rev.* A **93** 033402
[42] Grum-Grzhimailo A N, Gryzlova E V, Fritzsche S and Kabachnik N M 2016 *J. Mod. Opt.* **63** 334
[43] Gryzlova E V, Grum-Grzhimailo A N, Fritzsche S and Kabachnik N M 2010 *J. Phys. B: At. Mol. Opt. Phys.* **43** 225602
[44] Starace A 2006 Photoionization of atoms *Springer Handbook of Atomic, Molecular, and Optical Physics* ed G Drake (New York: Springer) p 379
[45] Yeh J J and Lindau I 1985 *At. Data Nucl. Data Tables* **32** 1
[46] Schippers S *et al* 2017 *Astrophys. J.* **849** 5
[47] Müller A *et al* 2021 *Phys. Rev.* A **104** 033105
[48] Grum-Grzhimailo A N 2001 *J. Phys. B: At. Mol. Opt. Phys.* **34** L359
[49] Hofbrucker J, Volotka A V and Fritzsche S 2020 *Sci. Rep.* **10** 3617
[50] Böning B, Paufler W and Fritzsche S 2019 *Phys. Rev.* A **99** 053404
[51] Hofbrucker J, Volotka A V and Fritzsche S 2016 *Phys. Rev.* A **94** 0634 12
[52] Achiezer A I and Berestecky V B 1969 *Quantum Electrodynamics* (Moscow: Nauka)
[53] Hofbrucker J, Böning B, Volotka A V and Fritzsche S 2021 *Phys. Rev.* A **104** 013102
[54] Ma R *et al* 2013 *J. Phys. B: At. Mol. Opt. Phys.* **46** 164018
[55] Ye L, Rouxel J R, Asban S, Rösner B and Mukamel S 2019 *J. Chem. Theory Comput.* **15** 4180
[56] Seipt D, Müller R A, Surzhykov A and Fritzsche S 2016 *Phys. Rev.* A **94** 053420
[57] Baghdasaryan B, Böning B, Paufler W and Fritzsche S 2019 *Phys. Rev.* A **99** 023403
[58] Müller N *et al* 2006 *Phys. Rev.* B **74** 161401(R)
[59] Hernández F E and Rizzo A 2011 *Molecules* **16** 3315
[60] De Silva A H N *et al* 2021 *Phys. Rev. Lett.* **126** 023201
[61] Hofbrucker J, Volotka A V and Fritzsche S 2017 *Phys. Rev.* A **96** 013409
[62] Fano U 1985 *Phys. Rev.* A **32** 617
[63] Fritzsche S and Böning B 2022 *Phys. Rev. Res.* **4** 033031
[64] Fritzsche S 2019 *Comput. Phys. Commun.* **240** 1
[65] Skruszewicz S *et al* 2021 *Phys. Rev. Lett.* **115** 043001
[66] Faisal F H M 2008 *Strong Field Laser Physics* (Springer Series in Optical Sciences vol 134) ed T Brabec (New York: Springer)
[67] Böning B and Fritzsche S 2020 *Phys. Rev.* A **102** 053108
[68] Böning B, Paufler W and Fritzsche S 2017 *Phys. Rev.* A **96** 043423
[69] Venzke J, Becker A and Jaron-Becker A 2020 *Sci. Rep.* **10** 16164